Desalination and Water Treatment
www.deswater.com

doi: 10.5004/dwt.2023.30201

316 (2023) 356–362
December

Preparation and characterization of visible-light driven La/Mg co-doped ZnO photocatalyst

Anukorn Phuruangrat[a,*], Titipun Thongtem[b,c], Somchai Thongtem[b,d,*]

[a]*Division of Physical Science, Faculty of Science, Prince of Songkla University, Hat Yai, Songkhla 90112, Thailand, Tel.: +66 (0)74 288374; Fax: +66 (0)74 288395; email: phuruangrat@hotmail.com (A. Phuruangrat)*
[b]*Materials Science Research Center, Faculty of Science, Chiang Mai University, Chiang Mai 50200, Thailand, Tel.: +66 (0)53 941915; Fax: +66 (0)53 941915; emails: schthongtem@yahoo.com (S. Thongtem), ttpthongtem@yahoo.com (T. Thongtem)*
[c]*Department of Chemistry, Faculty of Science, Chiang Mai University, Chiang Mai 50200, Thailand*
[d]*Department of Physics and Materials Science, Faculty of Science, Chiang Mai University, Chiang Mai 50200, Thailand*

Received 5 August 2023; Accepted 3 December 2023

ABSTRACT

ZnO and $La_xMg_{0.03-x}Zn_{0.97}O$ (x = 0.01, 0.015 and 0.02) nanoparticles prepared by combustion method were used for photocatalytic degradation of methylene blue (MB) as a dye model under visible light irradiation. Phase, morphology, surface area and optical properties of the samples were characterized by X-ray diffraction, transmission electron microscopy, Fourier-transform infrared spectroscopy, Raman spectroscopy, Brunauer–Emmett–Teller surface area analysis and UV-Visible spectrometry. The samples were indexed to pure hexagonal wurtzite ZnO nanoparticles with average particle size 115.64 ± 41.13, 67.25 ± 15.54, 36.80 ± 11.74 and 19.32 ± 4.11 nm for ZnO, $La_{0.01}Mg_{0.02}Zn_{0.97}O$, $La_{0.015}Mg_{0.015}Zn_{0.97}O$ and $La_{0.02}Mg_{0.01}Zn_{0.97}O$ samples, respectively. UV-Visible spectroscopy of ZnO nanoparticles has excellent absorption in UV region of 380 nm which was shifted to 384 nm for $La_{0.02}Mg_{0.01}Zn_{0.97}O$ nanoparticles by the incorporation of La/Mg dopants into the ZnO matrix. The photocatalytic efficiencies of ZnO, $La_{0.01}Mg_{0.02}Zn_{0.97}O$, $La_{0.015}Mg_{0.015}Zn_{0.97}O$ and $La_{0.02}Mg_{0.01}Zn_{0.97}O$ nanoparticles for MB degradation were 10.90%, 92.33%, 96.01% and 97.10%, respectively. The $La_{0.02}Mg_{0.01}Zn_{0.97}O$ nanoparticles have the highest photocatalytic activity because La/Mg co-dopant played the role in suppressing electrons–holes recombination and enhancing the photocatalytic activity of ZnO nanoparticles induced by visible radiation.

Keywords: La/Mg co-doped ZnO nanoparticles; Wastewater treatment; Spectroscopy

1. Introduction

Recently, photocatalysis, an advanced oxidation process, has been used as a potential application for environmental treatment including water and air because it has the benefit of complete degradation of contaminants without the existence of secondary pollutants [1–6]. ZnO with a wide bandgap of 3.37 eV and high exciton binding energy at room temperature of 60 meV is an outstanding photocatalyst for degradation of toxic pollutants because it is cost-effective, non-toxic and chemical stable and has high electron mobility [2,7–10]. Moreover, the limited photocatalytic activity of ZnO for pollution treatment is the rapid recombination of charge carriers, low quantum efficiency and active involvement with only UV light [1,3,7]. The incorporation of metals in ZnO lattice is an interesting way to promote photocatalytic activity under visible radiation because the metallic dopants can lead to create energy level between its

* Corresponding authors.

valence and conduction bands. Thus, the recombination of photo-excited electrons and photo-induced holes of ZnO is suppressed [9,11–13]. For example, $Zn_{0.85}La_{0.05}Ce_{0.05}Dy_{0.05}O$ has the photodegradation of rhodamine B (RhB) higher than the un-doped ZnO because rare earth metal, an electron acceptor, can lead to produce oxygen vacancy and to enhance the separation of photo-excited electrons and photo-induced holes [14]. The Al/Er co-doped ZnO nanoparticles have excellent degradation of RhB, methylene blue (MB) and 4-nitrophenol (4-NP) under visible radiation because they have strong visible light absorption and effective electron–hole separation [15].

In this research, La/Mg co-doped ZnO nanoparticles prepared by a simple combustion method were evaluated for the degradation of MB under visible radiation. Structure, morphology and optical property of ZnO and La/Mg co-doped ZnO samples were investigated by X-ray diffraction (XRD), transmission electron microscopy (TEM), Fourier-transform infrared spectroscopy (FTIR), Raman spectroscopy and UV-Visible spectrometry. Brunauer–Emmett–Teller (BET) surface area of samples was analyzed. The photocatalytic test showed that La/Mg co-dopants played the role in improving visible-light catalytic activity of un-doped ZnO.

2. Experimental details

To prepare $La_xMg_{0.03-x}Zn_{0.97}O$ (x = 0.01, 0.015 and 0.02) nanoparticles, 0.01 mol $Zn(NO_3)_2{\cdot}6H_2O$ was dissolved in 25 mL ethanol with continued stirring. Subsequently, the mixed solutions of 25 mL ethanol containing 0.01–0.02 wt.% $La(NO_3)_3{\cdot}6H_2O$ and $Mg(NO_3)_2{\cdot}6H_2O$ were added to the Zn^{2+} solution. In addition, 0.001 mol of NaOH containing in 50 mL ethanol was added with continued magnetic stirring for 24 h. In the end, the solution system was filtered and the solid residue was washed with deionized water and ethanol and dried at 80°C for 24 h. The solid residue was further calcined at 600°C for 4 h in an electrical furnace to obtain the final ZnO and La/Mg co-doped ZnO samples. Phase, morphology and optical property of ZnO and La/Mg co-doped ZnO samples were analyzed by XRD, TEM, FTIR, Raman spectroscopy and UV-Visible spectroscopy. BET surface area analysis for specific surface area of samples was operated on a Micromeritics TriStar II 3020 analyzer.

The photodegradation of MB over ZnO and La/Mg co-doped ZnO nanoparticles was studied under visible radiation. Each 200 mg of ZnO and La/Mg co-doped ZnO nanoparticles containing in 200 mL 1 × 10^{-5} M MB solution was magnetically stirred in dark condition for 30 min. Then, the solution system was irradiated by visible light of 35 W xenon lamp and 5 mL of suspension solution was collected every 30 min interval. The suspension solution was centrifuged at 4,000 rpm for 10 min to separate the photocatalytic solid. The solution of MB after photocatalytic reaction was analyzed by UV-Visible spectroscopy at a maximum wavelength (λ_{max}) of 664 nm. The degradation' efficiency (%) was calculated by Eq. (1).

$$\text{Degradation efficiency}(\%) = \frac{C_0 - C_t}{C_0} \times 100 \quad (1)$$

where C_o and C_t are the contents of MB before and after visible light irradiation. The mineralization of MB over $La_{0.02}Mg_{0.01}Zn_{0.97}O$ nanoparticles analyzed by total organic carbon (TOC) content was also investigated by a TOC Analytik Jena GmbH - multi N/C 3100 analyzer (Konrad-Zuse-Strasse 1, 07745 Jena, Germany).

3. Results and discussion

Phase and structure of ZnO and La/Mg co-doped ZnO samples were characterized by XRD as the results shown in Fig. 1. XRD pattern of the un-doped sample was indexed to pure phase of hexagonal wurtzite ZnO structure and well matched with the JCPDS no. 36-1451 [16]. Thus, ZnO sample prepared by combustion method and followed by 600°C calcination for 4 h was pure good crystal. Comparing to the ZnO sample, the XRD patterns of La/Mg co-doped ZnO samples were indexed to hexagonal wurtzite ZnO structure of the JCPDS no. 36-1451 [16]. There were no detection of impurities such as La_2O_3 and MgO, and the hexagonal wurtzite ZnO structure was not changed even after La/Mg co-dopants were incorporated in ZnO matrix. They should be noted that the diffraction peaks of La/Mg co-doped ZnO samples were shifted with respect to those of the pure hexagonal wurtzite ZnO phase. They indicate that La/Mg ions were successfully substituted for Zn^{2+} ions of ZnO lattice. The XRD patterns of La/Mg co-doped ZnO samples were broadened as compared to the pure phase of hexagonal wurtzite ZnO. The crystallite size of ZnO was reduced due to the addition of La/Mg to ZnO lattice because the La/Mg co-dopants led to prevent the crystallite growth and change the crystallite size of ZnO host during the crystallization of La/Mg co-doped ZnO samples [17–19]. The introduction of La/Mg co-dopant played the role in inhibiting the growth of ZnO nanoparticles.

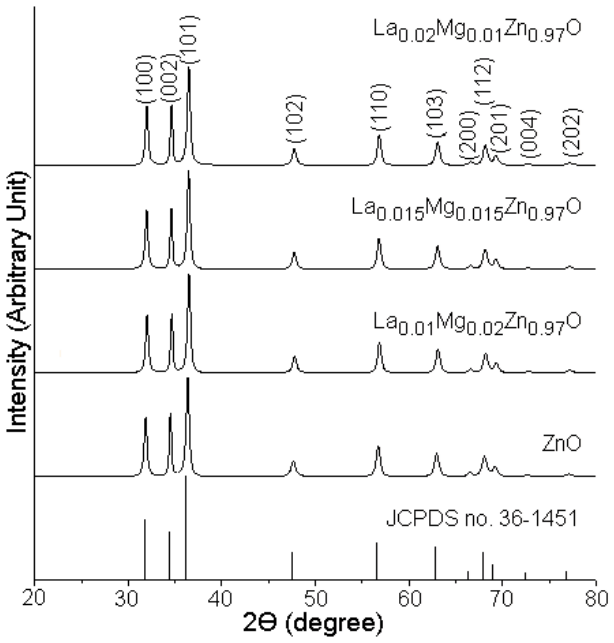

Fig. 1. X-ray diffraction patterns of ZnO and La/Mg co-doped ZnO samples as compared with the JCPDS database.

The approximate crystallite sizes of ZnO and La/Mg co-doped ZnO samples were calculated using the Scherrer Eq. (2).

$$D = \frac{k\lambda}{\beta\cos\theta} \quad (2)$$

where D is the approximate crystallite size of the sample, k is the Scherrer constant of spherical shape (k = 0.89), λ is the wavelength of Cu-Kα (λ = 0.154056 nm), θ is the Bragg diffraction angle of the (101) crystal plane of hexagonal wurtzite ZnO structure and β is the full width at half maximum of the (101) crystal plane [8,12,14,20–22]. The calculated crystallite sizes of ZnO, $La_{0.01}Mg_{0.02}Zn_{0.97}O$, $La_{0.015}Mg_{0.015}Zn_{0.97}O$ and $La_{0.02}Mg_{0.01}Zn_{0.97}O$ were 45.37, 29.91, 27.92 and 26.05 nm, respectively.

The atomic vibration of ZnO and La/Mg co-doped ZnO samples were investigated by FTIR and Raman spectroscopy. Fig. 2a shows the FTIR spectra of ZnO and $La_{0.015}Mg_{0.015}Zn_{0.97}O$ samples which present the sharp FTIR bands at 438 cm^{-1} for ZnO and 437 cm^{-1} for $La_{0.015}Mg_{0.015}Zn_{0.97}O$. They correspond to the vibration of Zn–O bond of ZnO lattice [3,4,8,12,13]. The wavenumber of Zn–O bond of La/Mg co-doped ZnO sample was slightly shifted with respect to that of pure ZnO sample due to the change of Zn–O bond length by the substitution of La/Mg co-dopants for Zn of ZnO [3,8,12,13]. The broad bands at 3,100–3,600 cm^{-1} were also detected and are assigned to the vibration of O–H stretching of adsorbed water on top of the samples [3,4,8,12,13].

Fig. 2b shows the Raman spectra of ZnO and $La_{0.015}Mg_{0.015}Zn_{0.97}O$ samples analyzed by He–Ne red laser at 632.8 nm in the wavenumber range of 200–700 cm^{-1}. Raman spectrum of pure ZnO phase shows the dominant Raman peak at 438 cm^{-1} which corresponds to the $E_{2(H)}$ mode of wurtzite ZnO structure [13,23,24]. The weak Raman peaks at 330 and 381 cm^{-1} of pure ZnO phase are assigned to the $E_{2(H)}$–$E_{2(L)}$ and $A_{1(TO)}$ modes of wurtzite ZnO structure [13,23,24]. The $E_{1(LO)}$ modes of wurtzite ZnO structure at 536 and 572 cm^{-1} are related to the lattice distortion and defects such as oxygen vacancy (V_O) and zinc interstitial (Zn_i) [13,23,24]. The wavenumber of $E_{2(H)}$ mode of wurtzite ZnO structure of La/Mg co-doped ZnO was slightly shifted to 437 cm^{-1} due to the disorder of ZnO lattice by La/Mg dopants in the ZnO host matrix [13,23–25]. They can be seen that the intensity of $E_{1(LO)}$ mode of wurtzite ZnO structure was increased after being doped with La/Mg because oxygen vacancy and defect were induced in ZnO lattice [13,20,24,26].

Fig. 3 shows TEM images and SAED (selected area electron diffraction) patterns of ZnO and La/Mg co-doped ZnO samples. Both ZnO and La/Mg co-doped ZnO samples contain spherical nanoparticles with different orientations. The particle size of ZnO was decreased when La/Mg co-dopants were incorporated in the ZnO lattice. The results show that growth rate of ZnO was suppressed. The average particle sizes were 115.64 ± 41.13, 67.25 ± 15.54, 36.80 ± 11.74 and 19.32 ± 4.11 nm for ZnO, $La_{0.01}Mg_{0.02}Zn_{0.97}O$, $La_{0.015}Mg_{0.015}Zn_{0.97}O$ and $La_{0.02}Mg_{0.01}Zn_{0.97}O$ samples, respectively. The particle size of La/Mg co-doped ZnO samples was decreased and the surface-to-volume ratio of ZnO was increased. The introduction of La/Mg co-dopant can lead to enhance the photocatalytic performance of the sample. The BET surface areas of ZnO and La/Mg co-doped ZnO samples were 14.13, 16.85, 18.10 and 19.76 m^2/g for ZnO, $La_{0.01}Mg_{0.02}Zn_{0.97}O$, $La_{0.015}Mg_{0.015}Zn_{0.97}O$ and $La_{0.02}Mg_{0.01}Zn_{0.97}O$ samples, respectively. The $La_{0.02}Mg_{0.01}Zn_{0.97}O$ nanoparticles have the highest active surface area for photocatalysis and visible-light harvest [27–29]. SAED patterns of ZnO and La/Mg co-doped ZnO samples present the full bright electron diffraction of concentric rings which indicate the existence of ZnO and La/Mg co-doped ZnO polycrystalline samples. The SAED patterns of un-doped and doped samples were indexed to the (100), (002), (101), (102) and (110) crystal planes of hexagonal wurtzite ZnO structure of the JCPDS no. 36-1451 [13]. The weight percentages of the elements containing in the $La_{0.02}Mg_{0.01}Zn_{0.97}O$ nanoparticles was analyzed by energy-dispersive X-ray spectroscopy and were 1.59% La, 0.73% Mg, 50.32% Zn and 47.36% O. They correspond very well with the molar percent of the elements containing in the sample.

Fig. 4 shows the UV-Visible absorption of ZnO and La/Mg co-doped ZnO samples in the wavelength range of ~220–800 nm. In this research, pure ZnO nanoparticles show excellent absorption in the UV region which is the

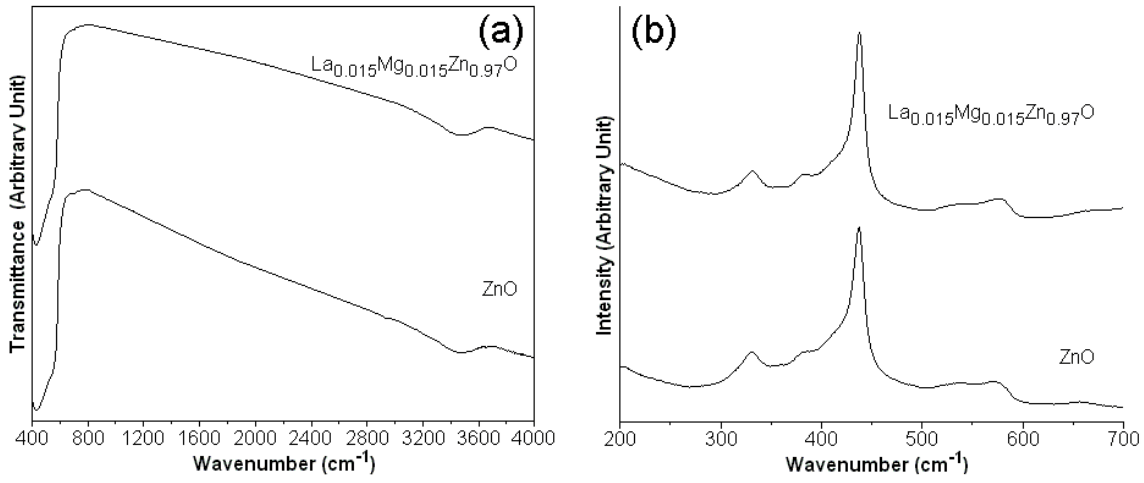

Fig. 2. (a) Fourier-transform infrared spectroscopy and (b) Raman spectra of ZnO and $La_{0.015}Mg_{0.015}Zn_{0.97}O$ samples.

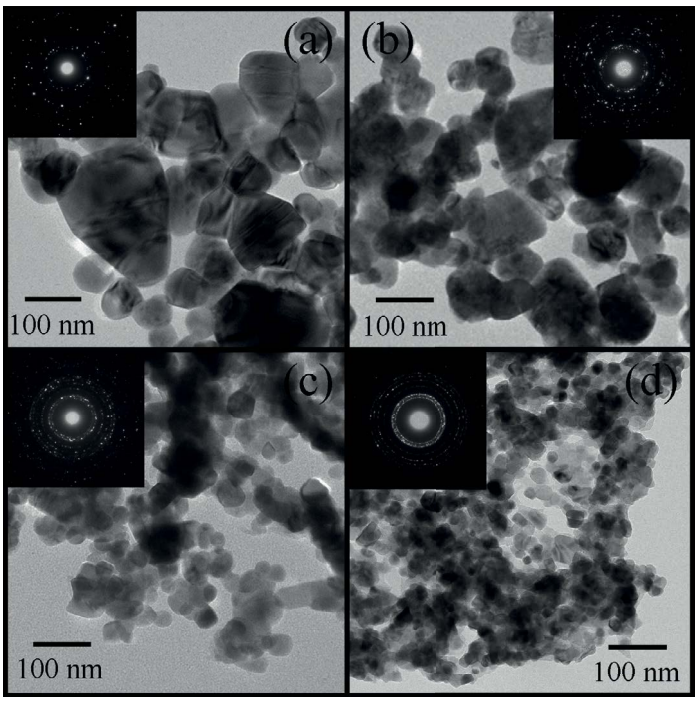

Fig. 3. Transmission electron microscopy images and SAED patterns of (a) ZnO, (b) $La_{0.01}Mg_{0.02}Zn_{0.97}O$, (c) $La_{0.015}Mg_{0.015}Zn_{0.97}O$ and (d) $La_{0.02}Mg_{0.01}Zn_{0.97}O$ nanoparticles.

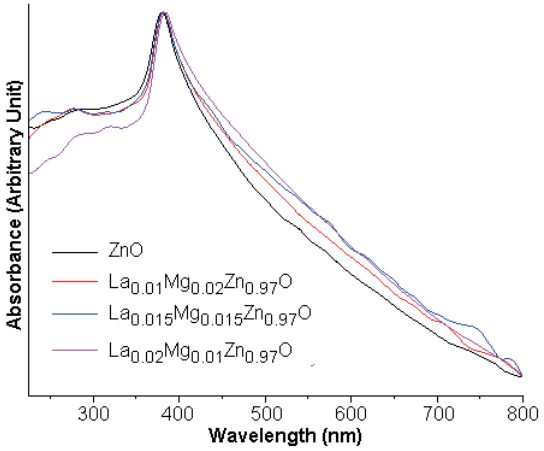

Fig. 4. Photonic absorption of ZnO and $La_xMg_{0.03-x}Zn_{0.97}O$ (x = 0.01, 0.015 and 0.02) nanoparticles.

characteristic of photo-induced charge carriers of wurtzite hexagonal ZnO structure [4,11,13,14]. When La/Mg co-dopants were incorporated into ZnO matrix, the visible absorption region was enlarged. Possibly, the impurity level in the band gap of ZnO can lead to improve the utilization of visible light [11,13,14,30]. The absorption edges of La/Mg co-doped ZnO nanoparticles were red shifted from 380 nm for ZnO nanoparticles to 381, 382 and 384 nm for $La_{0.01}Mg_{0.02}Zn_{0.97}O$, $La_{0.015}Mg_{0.015}Zn_{0.97}O$ and $La_{0.02}Mg_{0.01}Zn_{0.97}O$ nanoparticles, respectively. The band gaps (E_g) of ZnO and La/Mg co-doped ZnO nanoparticles were calculated using $E_g = 1{,}239.82/\lambda$. They were 3.26, 3.25, 3.24 and 3.23 eV for ZnO, $La_{0.01}Mg_{0.02}Zn_{0.97}O$, $La_{0.015}Mg_{0.015}Zn_{0.97}O$ and $La_{0.02}Mg_{0.01}Zn_{0.97}O$ nanoparticles, respectively [4,13,30,31]. The E_g of ZnO was reduced by the introduction of La/Mg co-dopants. The band gap narrowing mechanism is increasingly significant and is competing with the Burstein–Moss effect of ZnO [13,14,20,30,32]. The Burstein–Moss shift is a phenomenon that the apparent band gap of a semiconductor increases when the absorption edge is pushed to higher energy level as a result of all states close to the conduction band get populated.

Fig. 5a shows the photodegradation of MB over ZnO and La/Mg co-doped ZnO nanoparticles prepared by combustion method and followed by calcination at 600°C for 4 h. According to the results, the photodegradation of MB over ZnO under visible light irradiation within 90 min was 10.90%. The photocatalytic efficiency for MB degradation over ZnO was increased by being doped with La/Mg co-dopants. The La/Mg dopants have the influence on the photocatalytic reaction of ZnO under visible light irradiation. The photocatalytic efficiencies for MB degradation over La/Mg co-doped ZnO nanoparticles were 92.33%, 96.01% and 97.10% for $La_{0.01}Mg_{0.02}Zn_{0.97}O$, $La_{0.015}Mg_{0.015}Zn_{0.97}O$ and $La_{0.02}Mg_{0.01}Zn_{0.97}O$ nanoparticles, respectively. According to the present photocatalytic experiment, the $La_{0.02}Mg_{0.01}Zn_{0.97}O$ nanoparticles have the highest photocatalytic performance because they have the highest active surface area for photocatalytic reaction and incident visible light harvest to produce the highest active oxidant species as $^{\bullet}OH$ and $^{\bullet}O_2^-$ radicals for MB degradation under visible light irradiation [33–35]. The introduction of La/Mg co-dopant can lead to create oxygen vacancies and defects in ZnO lattice which plays the role in suppressing the recombination of photo-excited electrons – photo-induced holes and enhancing the photocatalytic performance of ZnO under visible light

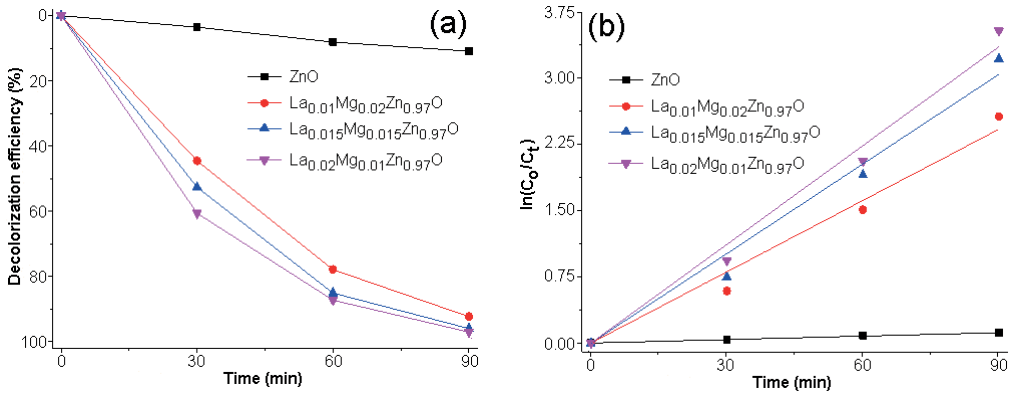

Fig. 5. (a) Photocatalysis and (b) $\ln C_o/C_t$ vs. irradiation time plots of ZnO and La/Mg co-doped ZnO nanoparticles for the degradation of methylene blue illuminated by visible radiation.

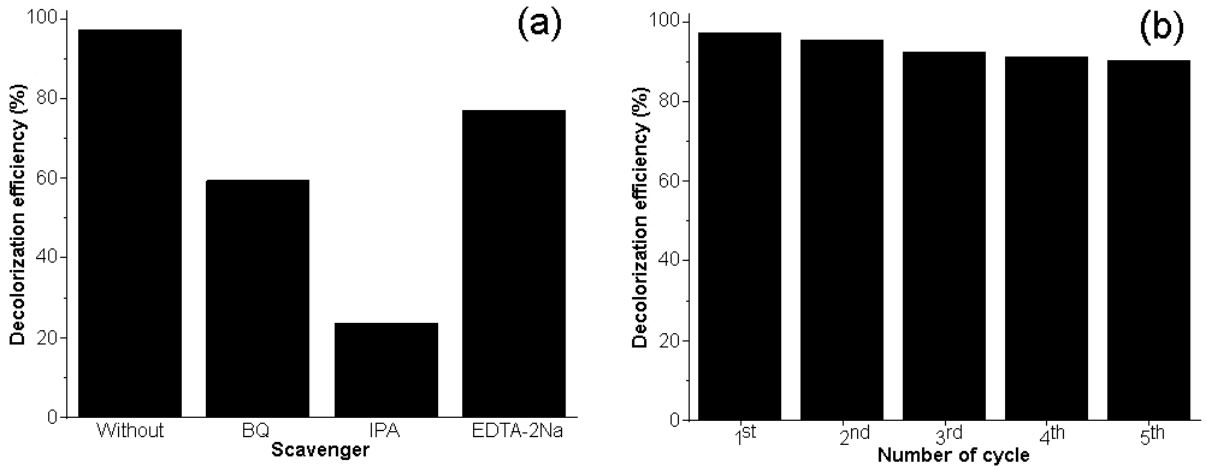

Fig. 6. (a) Trapping experiment and (b) recycled test of $La_{0.02}Mg_{0.01}Zn_{0.97}O$ nanoparticles for the degradation of methylene blue.

irradiation [1,8,36,37]. In addition, the mineralization of MB over $La_{0.02}Mg_{0.01}Zn_{0.97}O$ nanoparticles analyzed by TOC was 63.87%. The reaction kinetics for photodegradation of MB over ZnO and La/Mg co-doped ZnO nanoparticles follows the pseudo-first-order kinetics model of Fig. 5b [3,8,11,13,38–40]. They show linear lines of $\ln(C_o/C_t)$ vs. irradiation time with regression coefficient closed to 1. The apparent rate constant for MB degradation over a photocatalyst was calculated from the slope of $\ln(C_o/C_t)$ vs. irradiation time. The apparent rate constants for MB degradation were 1.67×10^{-3}, 0.0269, 0.0339 and 0.0374 min^{-1} for ZnO, $La_{0.01}Mg_{0.02}Zn_{0.97}O$, $La_{0.015}Mg_{0.015}Zn_{0.97}O$ and $La_{0.02}Mg_{0.01}Zn_{0.97}O$ nanoparticles, respectively. The $La_{0.02}Mg_{0.01}Zn_{0.97}O$ nanoparticles have the highest apparent rate constant.

Fig. 6a shows the degradation of MB over $La_{0.02}Mg_{0.01}Zn_{0.97}O$ nanoparticles with and without adding of ethylenediaminetetraacetic acid disodium salt (EDTA-2Na), isopropyl alcohol (IPA) and benzoquinone (BQ) used for trapping of holes (h^+), hydroxyl radical ($^\bullet OH$) and superoxide anion radical ($^\bullet O_2^-$) [8,12,15,33,41]. The photocatalytic efficiencies for MB gradation were slightly decreased after being added with EDTA-2Na. The dramatic decrease of degradation efficiency for MB over $La_{0.02}Mg_{0.01}Zn_{0.97}O$ nanoparticles was detected after being doped with IPA and BQ. Thus, $^\bullet OH$ and $^\bullet O_2^-$ radicals played the important role in photodegrading of MB under visible light irradiation. In addition, the photocatalytic stability of $La_{0.02}Mg_{0.01}Zn_{0.97}O$ nanoparticles was investigated as the results shown in Fig. 6b. At the end of photocatalytic reaction, the $La_{0.02}Mg_{0.01}Zn_{0.97}O$ nanoparticles were centrifuged, washed with R.O. water and ethanol, and dried for the next photocatalytic cycle. The results show that the re-used $La_{0.02}Mg_{0.01}Zn_{0.97}O$ nanoparticles were still have high photocatalytic activity and that $La_{0.02}Mg_{0.01}Zn_{0.97}O$ nanoparticles are an excellent photocatalyst for practical treatment of wastewater.

4. Conclusions

ZnO and La/Mg co-doped ZnO nanoparticles were successfully synthesized by combustion method and followed by calcination at 600°C for 4 h. Phase of the as-prepared un-doped sample was pure hexagonal wurtzite ZnO structure. The La/Mg co-dopants were successfully substituted for Zn^{2+} ions of the lattice and played the role in inhibiting the growth of ZnO nanoparticles. The photocatalytic activities of ZnO and La/Mg co-doped ZnO nanoparticles were monitored through the degradation of MB under visible light irradiation. The $La_{0.02}Mg_{0.01}Zn_{0.97}O$ nanoparticles

have the highest photocatalytic activity because the La/Mg co-dopants played the role in suppressing the electrons-holes recombination and enhancing the photocatalytic activity of ZnO under visible light irradiation. In this research, the re-used $La_{0.02}Mg_{0.01}Zn_{0.97}O$ nanoparticles are the excellent photocatalyst within five cycles and have the promising photocatalytic application for wastewater treatment.

Acknowledgement

This research was supported by National Science, Research and Innovation Fund (NSRF) and Prince of Songkla University (Grant No. SCI6601194S).

References

[1] I. Ahmad, M.S. Akhtar, E. Ahmed, M. Ahmad, Facile synthesis of Pr-doped ZnO photocatalyst using sol–gel method and its visible light photocatalytic activity, J. Mater. Sci., 31 (2020) 1084–1093.
[2] A.L.T. Zheng, C.A.C. Abdullah, E.L.T. Chung, Y. Andou, Recent progress in visible light-doped ZnO photocatalyst for pollution control, Int. J. Environ. Sci. Technol., 20 (2023) 5753–5772.
[3] R.M. Kakhki, R. Tayebee, F. Ahsani, New and highly efficient Ag doped ZnO visible nano photocatalyst for removing of methylene blue, J. Mater. Sci., 28 (2017) 5941–5952.
[4] S. Rabieh, K. Nassimi, M. Bagheri, Clew-like hierarchical ZnO nanostructure assembled by nanosheets as an efficient photocatalyst for degradation of azure B, J. Mater. Sci., 27 (2016) 10052–10058.
[5] M. Sabri, A. Habibi-Yangjeh, S.R. Pouran, C. Wang, Titania-activated persulfate for environmental remediation: the-state-of-the-art, Catal. Rev., 65 (2023) 118–173.
[6] S. Feizpoor, S.R. Pouran, A. Habibi-Yangjeh, Recent progress on photocatalytic evolution of hydrogen gas over TiO_{2-x}-based emerging nanostructures, Mater. Sci. Semicond. Process., 162 (2023) 107444, doi: 10.1016/j.mssp.2023.107444.
[7] L. Zhu, M. Zheng, J. Lu, M. Xu, H.J. Seo, Synthesis of CuS/ZnO nanocomposite and its visible-light photocatalytic activity, J. Nanomater., 2014 (2014) 126475, doi: 10.1155/2014/126475.
[8] N. Elamin, A. Modwi, M.A.B. Aissa, K.K. Taha, O.K. Al-Duaij, T.A. Yousef, Fabrication of Cr–ZnO photocatalyst by starch-assisted sol–gel method for photodegradation of Congo red under visible light, J. Mater. Sci., 32 (2021) 2234–2248.
[9] M. Hosseini-Sarvari, A.M. Sarvestani, N-doped ZnO as an efficient photocatalyst for thiocyanation of indoles and phenols under visible-light, Photochem. Photobiol. Sci., 20 (2021) 903–911.
[10] P.C. Nethravathi, D. Suresh, Silver-doped ZnO embedded reduced graphene oxide hybrid nanostructured composites for superior photocatalytic hydrogen generation, dye degradation, nitrite sensing and antioxidant activities, Inorg. Chem. Commun., 134 (2021) 109051, doi: 10.1016/j.inoche.2021.109051.
[11] D. Zhang, F. Zeng, Visible light-activated cadmium-doped ZnO nanostructured photocatalyst for the treatment of methylene blue dye, J. Mater. Sci., 47 (2012) 2155–2161.
[12] D. Laokae, A. Phuruangrat, T. Thongtem, S. Thongtem, Synthesis, analysis and visible-light-driven photocatalysis of 0–5% Pr-doped ZnO nanoparticles, Russ. J. Inorg. Chem., 67 (2022) 721–731.
[13] S. Sa-nguanprang, A. Phuruangrat, K. Karthik, S. Thongtem, T. Thongtem, Tartaric acid-assisted precipitation of visible light-driven Ce-doped ZnO nanoparticles used for photodegradation of methylene blue, J. Aust. Ceram. Soc., 56 (2020) 1029–1041.
[14] S. Irtiqa, A. Rahman, Photocatalytic and photoluminescence studies of La, Ce, and Dy co-doped ZnO nanoflowers, J. Inst. Eng. India Ser. E, 103 (2022) 259–270.
[15] U. Alam, A. Khan, W. Raza, A. Khan, D. Bahnemann, M. Muneer, Highly efficient Y and V co-doped ZnO photocatalyst with enhanced dye sensitized visible light photocatalytic activity, Catal. Today, 284 (2017) 169–178.
[16] Powder Diffract. File, JCPDS-ICDD, 12 Campus Blvd., Newtown Square, PA 19073-3273, U.S.A., 2001.
[17] H.S. Lokesha, A.R.E. Prinsloo, P. Mohanty, C.J. Sheppard, Impact of Cr doping on the structure, optical and magnetic properties of nanocrystalline ZnO particles, J. Alloys Compd., 960 (2023) 170815, doi: 10.1016/j.jallcom.2023.170815.
[18] N.M. Moussa, F.M. Ebrahim, K. Adly, M.Y. Hassaan, Chromium doped ZnO nanoparticles for energy storage, gas and humidity sensing and spin based electronic devices applications, Opt. Quantum Electron., 54 (2022) 683, doi: 10.1007/s11082-022-04075-y.
[19] M.M. Hassan, W. Khan, A. Azam, A.H. Naqvi, Effect of size reduction on structural and optical properties of ZnO matrix due to successive doping of Fe ions, J. Lumin., 145 (2014) 160–166.
[20] X. Zhang, M. Li, L. Li, L. Hu, S. Li, Effect of cerium doping on the textural, structural and antibacterial properties of zinc oxide, Russ. J. Inorg. Chem., 66 (2021) 2027–2035.
[21] S. Goel, N. Sinha, H. Yadav, A.J. Joseph, B. Kumar, 2D porous nanosheets of Y-doped ZnO for dielectric and ferroelectric applications, J. Mater. Sci., 29 (2018) 13818–13832.
[22] P.C. Nethravathi, Udayabhanu, G. Nagaraju, D. Suresh, TiO_2 and Ag-TiO_2 nanomaterials for enhanced photocatalytic and antioxidant activity: green synthesis using *Cucumis melo* juice, Mater. Today: Proc., 49 (2022) 841–848.
[23] Z.Y. Jiang, K.R. Zhu, Z.Q. Lin, S.W. Jin, G. Li, Structure and Raman scattering of Mg-doped ZnO nanoparticles prepared by sol–gel method, Rare Met., 37 (2018) 881–885.
[24] N. Ekthammathat, A. Phuruangrat, T. Phonkhokkong, W. Maisang, P. Junploy, A. Klinbumrung, S. Thongtem, T. Thongtem, Sonochemical synthesis, characterization, and magnetic properties of Mn-doped ZnO nanostructures, Rare Met., 40 (2021) 3561–3566.
[25] L. Umaralikhan, M.J.M. Jaffar, Green synthesis of ZnO and Mg doped ZnO nanoparticles, and its optical properties, J. Mater. Sci., 28 (2017) 7677–7685.
[26] Q. Gao, Y. Dai, X. Li, L. Yang, C. Cui, C. Li, Effects of Mn dopant on tuning carrier concentration in Mn doped ZnO nanoparticles synthesized by co-precipitation technique, J. Mater. Sci., 29 (2018) 3568–3575.
[27] T. Rungsawang, S. Sujinnapram, S. Nilphai, S. Wongrerkdee, Influence of yttrium doping on ZnO nanoparticles for enhanced photocatalytic degradation of methylene blue, Dig. J. Nanomater. Biostruct., 16 (2021) 1209–1217.
[28] M. Naeem, S. Qaseem, I.H. Gul, A. Maqsood, Study of active surface defects in Ti doped ZnO nanoparticles, J. Appl. Phys., 107 (2010) 124303, doi: 10.1063/1.3432571.
[29] P.C. Nethravathi, M.V. Manjula, S. Devaraja, D. Suresh, Ag and $BiVO_4$ decorated reduced graphene oxide: a potential nano hybrid material for photocatalytic, sensing and biomedical applications, Inorg. Chem. Commun., 139 (2022) 109327, doi: 10.1016/j.inoche.2022.109327.
[30] I. Ahmad, E. Ahmed, M. Ullah, A.M. Rana, M.F. Manzoor, M.A. Rasheed, A.S. Malik, N.R. Khalid, M. Ahmad, U. Mehtab, Synthesis and characterization of silver doped ZnO nanoparticles for hydrogen production, J. Ovonic Res., 14 (2018) 415–427.
[31] B.A. Bader, N.H. Numan, F.G. Khalid, M.A. Fakhri, A.W. Abdulwahhab, Effects of substrate temperatures on optical properties and constants of ZnO prepared by PLD, J. Ovonic Res., 15 (2019) 127–133.
[32] P. Raju, D. Deivatamil, J.A.M. Mark, J.P. Jesuraj, Antibacterial and catalytic activity of Cu doped ZnO nanoparticles: structural, optical, and morphological study, J. Iranian Chem. Soc., 19 (2022) 861–872.
[33] P. Zhang, B. Liu, Y. Li, N. Chen, Y. Du, W. Chang, H. Yang, W. Hong, Y. Li, G. Yang, Egg white-mediated synthesis and application of Ag/CeO_2 photocatalyst for enhanced

photocatalytic activity under visible light irradiation, Russ. J. Inorg. Chem., 66 (2021) 2036–2044.
[34] J. Sakfali, S.B. Chaabene, R. Akkari, M.S. Zina, One-pot sol–gel synthesis of doped TiO_2 nanostructures for photocatalytic dye decoloration, Russ. J. Inorg. Chem., 67 (2022) 1324–1337.
[35] S.S. Mohtar, F. Aziz, A.F. Ismail, N.S. Sambudi, H. Abdullah, A.N. Rosli, B. Ohtani, Impact of doping and additive applications on photocatalyst textural properties in removing organic pollutants: a review, Catalysts, 11 (2021) 1160, doi: 10.3390/catal11101160.
[36] S. Irtiqa, A. Rahman, Photocatalytic studies of La, Ce co-doped ZnO nanoparticles, Russ. J. Appl. Chem., 93 (2020) 1906–1919.
[37] X. Zhu, L. Pei, R. Zhu, Y. Jiao, R. Tang, W. Feng, Preparation and characterization of Sn/La co-doped TiO_2 nanomaterials and their phase transformation and photocatalytic activity, Sci. Rep., 8 (2018) 12387, doi: 10.1038/s41598-018-30050-3.
[38] M.S. Azmina, R.M. Nor, H.A. Rafaie, S.F.A. Sani, Z. Osman, Enhanced photocatalytic performance of silver decorated zinc oxide nanoparticles grown on silica microparticles, Silicon, 11 (2019) 2845–2852.
[39] J. Tang, R. Meng, Y. Xue, S. Zhang, Q. Li, Fabrication of a novel $Ag_3PO_4/WO_3{\cdot}H_2O$ composite with enhanced visible light photocatalytic performance for the degradation of methylene blue and oxytetracycline, Inorg. Chem. Commun., 132 (2021) 108792.
[40] L. Mohanty, D.S. Pattanayak, R. Singhal, D. Pradhan, S.K. Dash, Enhanced photocatalytic degradation of rhodamine B and malachite green employing $BiFeO_3$/g-C_3N_4 nanocomposites: an efficient visible-light photocatalyst, Inorg. Chem. Commun., 138 (2022) 109286, doi: 10.1016/j.inoche.2022.109286.
[41] X. Li, X. Feng, R. Li, W. Liu, Adsorption and photocatalytic properties of titanium dioxide/chitosan/bentonite composites for methylene blue, Russ. J. Inorg. Chem., 67 (2022) S98–S113.